Fault Diagnosis of the Four-Rotor Unmanned Aerial Vehicle using the Optimized Deep Forest Algorithm based on the Wavelet Packet Translation

Shaojie Ai
School of Astronautics (of Beihang University)
Beijing, China
aishaojie@buaa.edu.cn

Weize Shang
School of Astronautics (of Beihang University)
Beijing, China
shangwz0918@163.com

Jia Song
School of Astronautics (of Beihang University)
Beijing, China
songjia@buaa.edu.cn

Guobiao Cai
School of Astronautics (of Beihang University)
Beijing, China
cgb@buaa.edu.cn

***Abstract*—In this paper, the diagnostic issues for the four-rotor unmanned aerial vehicle (UAV) with the sensor fault, the actuator fault and the composite fault are considered. Existing data-driven methods mostly present drawbacks of structural complexity and insufficient generalization ability. Therefore, a novel fault diagnosis scheme based on the optimized deep forest (GcForest) algorithm is put forward. According to the flight mission and mechanism of the four-rotor UAV, the six-degree-of-freedom model and fault database are established. First, the wavelet packet translation (WPT) is used for fault feature extraction. Second, the fault isolation process is achieved by the GcForest algorithm. While the optimal cascade forest internal structure parameter is obtained by the grid search optimizer. Finally, simulation studies are provided to illustrate the enhanced performance and efficiency of the proposed approach. In addition, to solve the difficulty of diagnosis with a small number of samples, simulation experiments based on multiple working conditions are performed to evaluate the generalization capability.**

Keywords: fault diagnosis, four-rotor unmanned aerial vehicle, deep forest, wavelet packet translation, composite fault

I. Introduction

Unmanned aerial vehicle (UAV) is a type of vehicle operated by wireless remote control and the self-provided program [1]. Among them, four-rotor UAV is widely used in agriculture, logistics, rescue, and other civil fields [2] due to its simple structure, hovering capability, and good dynamic performance [3]. The four-rotor UAV is intended for frequent, long-term, high-intensity missions. Furthermore, strong vibrations and multiple disturbances are the main characteristics of its working environment [4]. Therefore, when flying off the ground, sensors and actuators are prone to faults [5]. This will seriously affect the flight performance of the four-rotor UAV, causing aircraft instability, body damage, and even casualties. Failure diagnosis research is very important for the stability and reliability of the four-rotor UAV.

The four-rotor UAV is a nonlinear and strongly coupled under-fitting system. With the rapid development of computer technology and electronic materials technology, the composition and design of devices are becoming increasingly complex [6]. In the process of repeated high-intensity operation for a long time, the high-speed and high-load operation of the actuator may cause structural damage [7]. Due to the limited volume of aircraft, highly coupled micro-electronic sensors are vulnerable to vibration, leading to failure [8]. Under the real working condition, faults often have the characteristics of concurrency and affiliation, which cause uncertain composite faults. In order to guide researchers in improving the flight performance of four-rotor UAVs with fault-tolerant control, faults must be detected in an effective and timely manner. Hence, efficient and accurate fault diagnosis methods are urgently needed [9].

Fault diagnosis methods for complex nonlinear systems can be divided into analytical model-based methods and data-driven methods [10]. The former is supported by precise mathematical models and extensive expert experience [11]. There are difficulties with the accuracy guarantee. The accurate mathematical model of the complex system is generally difficult to obtain. And system error, noise and interference are difficult to model with precision. While the latter does not depend on the system modelling accuracy. The artificial intelligence (AI) technology is used to learn massive historical data, and diagnose directly by the system monitoring status information [12]. Based on the above analysis, data-driven

This work was supported by the National High-Tech Research and Development Program of China under Grants Nos.11100002017115004, 111GFTQ2018115005 and 111GFTQ2019115006, the National Natural Science Foundation of China under Grants 61473015, 91646108 and 62073020, and the Space Science and Technology Foundation of China under Grant 105HTKG2019115002. The authors thank the colleagues for their constructive suggestions and research assistance throughout this study. The authors also appreciate the associate editor and the reviewers for their valuable comments and suggestions.

22767-6684/21/$31.00 ©2021 IEEE
DOI 10.1109/DSA52907.2021.00085

methods are suitable for the fault diagnosis of the four-rotor UAV with complex structure and uncertain flying environment.

The data-driven fault diagnosis is realized in two steps: fault feature extraction and fault isolation. The sensitivity of the features significantly affects the effectiveness of the fault diagnosis [13]. In order to obtain state's hidden feature information, scholars in the field have used amount of signal processing methods to analyze the signals of the system state. H. Wang et al. [14] extracted the fault characteristics using a Bayesian network and a compressive sensing algorithm. M. Kordestani et al. [15] used discrete wavelet transformation (DWT) to extract features of the controller and sensor signal to the multifunctional spooler system, and provided guidance to ANN in recognizing faults. Z. Jin et al. [16] realized the intelligent fault diagnosis of rolling bearings by combining Welch power spectrum analysis and radial basis function natural network. Y. Li et al. [17] proposed hierarchical symbol dynamic entry (HSDE) method to extract the fault information in the high frequency components, and improve the classification effect of binary tree support vector machine (BT-SVM). Accordingly, the following conclusions are reached: (1) advanced signal processing technology can realize the extraction of sensitive features; (2) the selection of appropriate fault features can improve the fault isolation performance of the subsequent classifier.

After obtaining the fault features of the observed signals, AI learning machines are widely used for fault isolation. D. Guo et al. [18] combined the short time Fourier transform (STFT) with the convolution neural network (CNN) to identify sensor faults of the UAV. Compared to the neural network based method, the random forest (RF) has become a research hotspot for its less hyper-parameters, stronger robustness and no over-fitting. S. Ma et al. [19] developed a fault identification system for the high voltage circuit breaker (HVCB), based on the WPT and RF. However, the weight-sharing feature of the decision-making process causes a degradation of generalization performance. With this in mind, Z. Zhou et al. [20] proposed the GcForest algorithm in 2017. It is a supervised machine learning algorithm based on the RF and deep neural network (DNN). An excellent representation and learning ability, the adaptive model complexity adjustment mechanism grant superiority to GcForest. G. Hu et al. [21] applied the combination of GcForest and deep boltzmann machine (DBM) for industrial fault diagnosis, and proved that it has better isolation accuracy than deep learning (DL). Q. Liu et al. [22] conducted the small-sample fault diagnosis model of rolling bearing using the GcForest algorithm. However, for the four-rotor UAV fault signal, the high temporal correlation and large noise interference make it insufficient to analyze signals in time domain. WPT can extract sensitive time-frequency features by calculating the energy distribution, but it also brings the problem of feature impoverishment. If the feature set to be selected is too small, RF may rely heavily on one feature and ignore the sensitivity contribution of others. The biggest advantage of GcForest is that it greatly increases the number and diversity of selected features through multi-grained scanning. Moreover, the sensitivity of selected features is further enhanced by cascade forest. It can be said that the dual promotion of feature sensitivity and diversity has been realized from twofold of width and depth.

The flight of four-rotor UAV is with changeable attitude, rich fault forms and small training data. In summary, GcForest algorithm is introduced in this work, aiming to achieve high-precision fault diagnosis and improve the generalization ability of the algorithm. The state information obtained by four-rotor UAV is continuous signals. Certain amount of feature information is lost during the transmission in the cascade forest of GcForest, which leads to the decline of classification performance. Although adding more cascade forest layers can reduce the feature dilution, the classification time increases exponentially. Therefore, the energy feature of state signals is extracted by the WPT, and the dimension of input data is reduced, solving the above problems. Furthermore, the classification of GcForest depends on the setting of the internal structure parameters of the cascade forest to some extent. In order to get the optimal fault diagnosis model under the same fault pattern, the Grid Search algorithm is used to optimize the structural parameters of forest in this paper.

The contributions and highlights of this paper are summarized twofold:

1) *Combination of the WPT and GcForest algorithm is proposed for fault diagnosis of the four-rotor UAV.*
2) *Optimal GcForest-based fault diagnosis model is automatic constructed by Grid Search optimization.*

The rest of this paper is organized as follows. Section II describes the established four-rotor UAV mathematical model, attitude control model, sensor fault model, actuator fault model and composite fault model. Section III gives the specific scheme of the proposed optimized GcForest-WPT fault diagnosis of the four-rotor UAV. Section IV evaluates the performance of the method from simulation experiments. Conclusion is summarized in Section V.

II. Four-rotor UAV model with Faults

A. Four-rotor UAV Model

The following hypotheses are used to establish the mathematical model: (1) the four-rotor UAV is a rigid body; (2) the center of gravity of the aircraft coincides with the geometric center; (3) the acceleration of gravity is a consistent value; (4) the ground coordinate system coincides with the inertial system. The four-rotor UAV has an "X" rigid body structure composed of four brushless DC motors and fixed propellers, as shown in Fig. 1.

In the figure, the body coordinate system is defined as follows. The origin O is taken as the center of mass. The x_b axis is parallel to the body and points toward the nose. The y_b axis is perpendicular to the body and points to the right. The z_b axis is perpendicular to the x_b - y_b plane and points downwards.

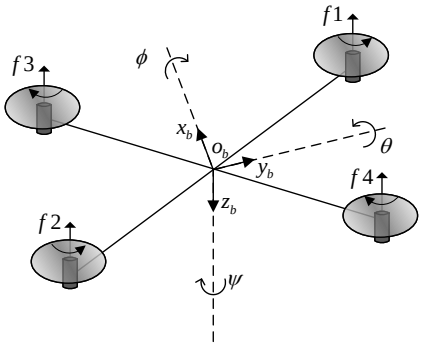

Fig. 1. The body fix reference frame of the four-rotor UAV.

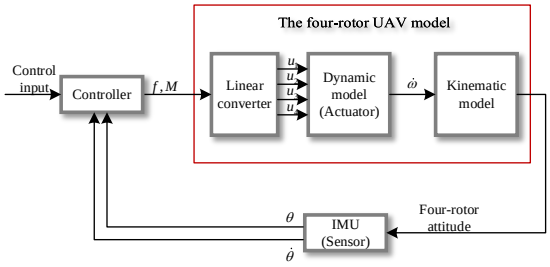

Fig. 2. Four-Rotor UAV controller topology.

The mathematical model of four-rotor UAV consists of dynamic equation and kinematic equation, and its six-degree of freedom model is described by the following equations:

$$\dot{\phi} = p + \sin\phi\tan\theta + \cos\phi\tan\theta \tag{1}$$

$$\dot{\theta} = q\cos\phi - r\sin\phi \tag{2}$$

$$\dot{\psi} = q\sin\phi\sec\theta + r\cos\phi\sec\theta \tag{3}$$

$$\ddot{x} = U_1(\sin\theta\cos\psi\cos\phi + \sin\psi\sin\phi)/m - D_z\dot{x}^2/m \tag{4}$$

$$\ddot{y} = U_1(\sin\theta\sin\psi\cos\phi - \cos\psi\sin\phi)/m - D_y\dot{y}^2/m \tag{5}$$

$$\ddot{z} = \left[U_1\cos\theta\cos\phi - D_z\dot{z}^2\right]/m - g \tag{6}$$

where (x, y, z) represents the coordinates of the center of mass of the vehicle under the earth coordinate system. θ, ϕ and ψ are the pitch, roll and yaw angle, respectively. D_x, D_y and D_z are air resistance coefficients of three axes. p, q, r represent rotation angular velocity of under the body coordinate system, which are formulated as follows:

$$\dot{p} = (J_r - J_z)qr/J_x + \left[j_r(-\omega_1 + \omega_2 - \omega_3 + \omega_4) + U_2\right]/J_x \tag{7}$$

$$\dot{q} = (J_z - J_x)pr/J_y - \left[j_r(-\omega_1 + \omega_2 - \omega_3 + \omega_4) + U_3\right]/J_y \tag{8}$$

$$\dot{r} = \left[(J_x - J_y)pq + U_4\right]/J_z \tag{9}$$

where J_x, J_y and J_z refer to the rotational inertia of the body. j_r refers to the rotational inertia of the rotor. U_2, U_3 and U_4 represent the aerodynamic moment. ω_1, ω_2, ω_3 and ω_4 are the rotor speed.

After the vehicle mathematics model is completed, the flow of the control system is established as shown in Fig. 2. The system is comprised primarily of the controller, actuator, sensor and four-rotor UAV unit. Among them, the actuator is the brushless DC motor, and the sensor is the Inertial Measurement Unit (IMU) composed of accelerometer and gyroscope.

B. Sensor Fault Model

To better control the attitude, it is necessary to observe the pitch angle and angular velocity. Therefore, typical sensor fault modeling of the angle sensor (accelerometer) is listed in TABLE I and carried out as follows:

$$\begin{pmatrix}\theta_1\\ \theta_2\\ \theta_3\\ \theta_4\end{pmatrix} = \left[\begin{pmatrix}1&0&0&0\\0&0&0&0\\0&0&k_1&0\\0&0&0&1\end{pmatrix}\cdot F^{\theta}_{4\times1} + \begin{pmatrix}\alpha_1\\ \alpha_2\\ 0\\ \delta_1(t_0)\end{pmatrix}\right]\cdot\beta(t-t_0) + F^{\theta}_{4\times1}\cdot\beta(t_0-t) \tag{10}$$

where $F^{i}_{m\times n}$ is a matrix whose elements are all equal to i, and with dimension of $m \times n$. $\beta(t) = 0.5(\mathrm{sgn}(t)+1)$ is the fault time profile function. $\delta_i(t)$ is a shock signal. t_0 represents the fault injection time.

The rate gyroscope is an important aerial sensor that provides an angular velocity signal to the navigation and guidance system. In order to ensure an accurate measurement, the angular rate sensor fault model is established as follows:

$$\begin{pmatrix}\dot{\theta}_1\\ \dot{\theta}_2\\ \dot{\theta}_4\end{pmatrix} = \left[\begin{pmatrix}1&0&0\\0&0&0\\0&0&1\end{pmatrix}\cdot F^{\dot{\theta}}_{3\times1} + \begin{pmatrix}\alpha_1\\ \alpha_2\\ 0\\ \delta_2(t_0)\end{pmatrix}\right]\cdot\beta(t-t_0) + F^{\theta}_{3\times1}\cdot\beta(t_0-t) \tag{11}$$

Generally, the data-deviation fault is a constant bias value added to the normal signal. The performance of stuck fault maintains a constant and noiseless value. Gain-changed fault shows that the deviation between the fault signal and normal signal increases gradually. The outlier-data fault appears to be a large point of deviation in an instant.

TABLE I
TYPICAL FAULT PATTERNS AND TYPES OF THE FOUR-ROTOR UAV

	Pattern	Type	Causes
Sensor Fault	$\theta_1(\dot{\theta}_1)$	Data-deviation fault	Environment temperature instability causes the bias current and voltage drifting in the amplifier circuit.
	$\theta_2(\dot{\theta}_2)$	Stuck fault	Permanent damage of the sensor cased by high overload operation.
	θ_3	Gain-changed fault	The dielectric constant and sensitivity changes at the high temperature [23].
	$\theta_4(\dot{\theta}_4)$	Outlier-data fault	Extreme weather aggravates the body and causes the local shock wave.
Actuator Fault	ω_1	Constant deviation fault	Harmonic current caused by the high-frequency switch leads to voltage distortion [24].
	ω_2	Complete failure	In the high-speed cases, the rotor runs out of phase and burns down afterwards.
	ω_3	Thrust decline fault	The resistance value of the potentiometer changes when the high-speed rotating rotor generates heat [25].
	ω_4	Abrupt thrust change	The local current is produced by the conductive particles in the strong polluted environment.

C. Actuator Fault Model

Brushless DC motors are used on the four-rotor UAV, driving the propeller to generate tension. The performance of actuator fault in speed signal is the same as sensor fault. In particular, the complete failure signal maintained 0. If the actuator fails, the system will be unable to respond to the control signal. Consequently, the following actuator fault model is listed in TABLE I and established:

$$\begin{pmatrix} \omega_1 \\ \omega_2 \\ \omega_3 \\ \omega_4 \end{pmatrix} = \left[\begin{pmatrix} 1 & 0 & 0 & 0 \\ 0 & 0 & 0 & 0 \\ 0 & 0 & k_2 & 0 \\ 0 & 0 & 0 & 1 \end{pmatrix} \cdot F^{\omega}_{4\times 1} + \begin{pmatrix} c_1 \\ 0 \\ 0 \\ \delta_3(t_0) \end{pmatrix} \right] \cdot \beta(t-t_0) + F^{\theta}_{4\times 1} \cdot \beta(t_0 - t) \quad (12)$$

It needs to be detailed that the motor speed signal can not be observed directly from the actual four-rotor UAV. When the motor breaks down, the change of tension has a direct impact on the angular acceleration. Therefore, the motor fault signal is observed in this paper through the angular rate sensor. Additionally, it should be noted that the above fault pattern is considered with the single actuator.

D. Composite fault model

The angular rate sensor fault and the motor fault influence and cover each other. In order to solve the problem that it is difficult to distinguish both when occurred at once, the composite fault model is formed as follows:

$$\begin{cases} u_1 = \begin{pmatrix} \dot{\theta} & \omega_3 \end{pmatrix}^T \\ u_2 = \begin{pmatrix} \dot{\theta} & \omega_2 \end{pmatrix}^T \\ u_3 = \begin{pmatrix} \dot{\theta}_1 & \omega \end{pmatrix}^T \\ u_4 = \begin{pmatrix} \dot{\theta}_1 & \omega_2 \end{pmatrix}^T \\ u_5 = \begin{pmatrix} \dot{\theta}_1 & \omega_3 \end{pmatrix}^T \end{cases} \quad (13)$$

III. THE GCFORST-WPT BASED FAULT DIAGNOSIS METHOD

A. Overview of the GcForst-WPT Based Fault Diagnosis Scheme

In this section, the proposed fault diagnosis scheme for the four-rotor UAV is stated. The flow of the strategy is depicted in Fig. 3.

First, the four-rotor UAV attitude control system model in a software environment is simulated for acquiring the sample data set. The standard condition dataset is divided into the training set and testing set according at a certain rate. While the data obtained under test condition are only used to generate the testing set. Next, after the data preprocessing, all sample data are processed by the WPT, and the energy feature of the sample signal is calculated. Then, the fault isolation model is built by the GcForest algorithm, and the fault classification is performed using the extracted feature. Finally, according to the testing accuracy of the Gcforest-based classification network, the Grid Search algorithm is used to optimize the structural parameters of cascaded forest. After optimization, the optimum model for fault diagnosis of the four-rotor UAV is constructed.

B. Fault Dataset Establishment

When the four-rotor UAV simulation model is successfully constructed, the simulation models with various faults are also built. Under the standard working condition, the simulation

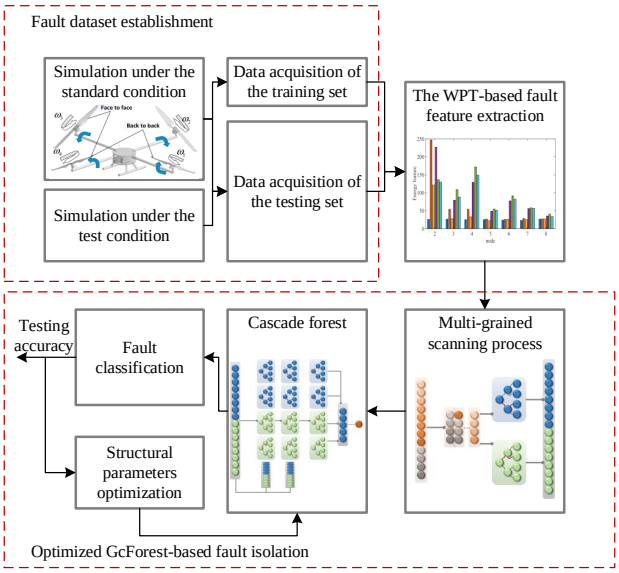

Fig. 3. Overview of the GcForst-WPT based fault diagnosis scheme for the four-rotor UAV.

program with sampling time T is run to obtain the angle and angular velocity signals in the normal and fault state. Depending on the fault injection time$t$ and performance time, sample points in $[t - t_a, t + t_b]$ are intercepted as a sample data. With the change in noise injection, the above operations are repeated N times to form the standard condition dataset. It is then divided into a training and testing set.

In particular, the normal state changes as the flying condition switches. Multiple test conditions are defined and corresponding dataset is generated. In practice, the increase of test conditions will lead to the doubling of the experimental cost. Therefore, the test condition dataset is only used to compose the test set.

C. The WPT-based Fault Feature Extraction Model

The four-rotor UAV sensor observation signal is a time sequence signal. The low-frequency part of the signal is the main information, while the high-frequency part contains the measurement noise and fault information. The above characteristics make fault diagnosis more difficult only on discrete sampling signal features in the time domain. In order to take into account the calculation burden reduction and classification accuracy of the GcForest, signal feature dimensions need to be reduced. In addition, sensitivity features should be retained as much as possible.

In order to better describe the fault information implicit in the sensor signal, the WPT is performed to analyze in the domain of time and frequency. The WPT can decompose the high and low frequency of each decomposition layer at the same time [26]. The discrete signal's WPT algorithm is expressed as below:

$$\begin{cases} d_l(j, 2n) = \sum_k a_{k-2l} d_k(j+1, n) \\ d_l(j+1, n) = \sum_k b_{k-2l} d_k(j+1, n) \end{cases} \tag{14}$$

where j is the number of decomposition layers, n is the number of decomposition bands, a_k and b_k are the decomposition coefficients. The energy of the signal $f(x)$ in time domain is expressed as:

$$\|f\|^2 = \int |f(x)|^2 \, \mathrm{d}x \tag{15}$$

The wavelet transform is performed on (15),the decomposition coefficient is expressed as:

$$d(j,k) = 2^{j/2} \int_R \overline{\phi(2^{-j}x - k)} f(x) \mathrm{d}x \tag{16}$$

where $\phi(x)$ is the wavelet basis function. Based on the Parseval equation, the relationship between (15) and (16) is expressed as:

$$\int_{-\infty}^{+\infty} |f(x)|^2 \, \mathrm{d}x = \int |d(j,k)|^2 \tag{17}$$

Derived from (17), square of the decomposition coefficient can be used as the energy feature of the signal.

Based on the above analysis, the time sequence data derived from the simulation experiment are then processed by the WPT. The energy distribution characteristics are obtained by calculating decomposition coefficients for different frequency bands. Therefore, the WPT-based fault feature extraction model is completed. Its output is passed into the following fault isolation model as input.

D. The fault isolation model based on the optimized GcForest

There are two stages involved in the classification process of the Gcforest algorithm: the multi-gained scanning and the cascade forest. The former is used to increase the dimension of sample features, while the latter is further needed to select features through multi-layer built by the random forest and completely random forest. Once the mapping relationship between features and labels is iteratively fitted, the classification results are displayed.

To some extent, the classification accuracy of Gcforest is dependent on the number of random forests and completely random forests and their internal structure parameters. The internal structure parameters are shown in TABLE II, which have the characteristics of small amount and high universality.

As the most traditional way of hyper-parameters tuning, the Grid Search algorithm enumerate every possible configurations in the search space to get the optimal hyperparameter setting [27]. Consequently, the Grid Search method is used to achieve automatic optimization of the adjustable parameters to build the optimal classification model. The work flow of the proposed fault isolation model establishment is depicted in Fig. 4.

The entire process can be split into two parts: training and testing. The specific steps are set out below.

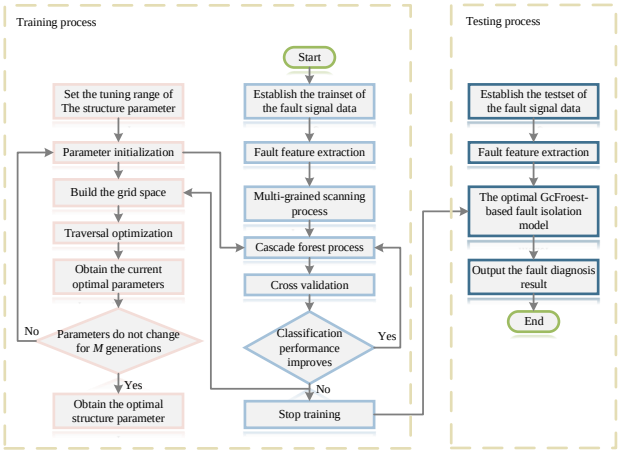

Fig. 4. Flow chart of the GcForest based fault isolation method.

TABLE II
THE INTERNAL STRUCTURE PARAMETER OF THE CASCADE FOREST

	Meaning	**Tuning$_a$ Range**
N_e	The number of decision trees in the forest	$(5, 40, 5)$
D_{max}	The maximum depth of the decision tree	$(1, 13, 2)$
S_{min}	The minimum number of samples required to split an internal node	$(30, 150, 20)$
L_{min}	The minimum number of samples required to be at a leaf node	$(5, 30, 5)$

[a] (a, b, i) is a range value of minimum a,maximum b and interval i.

1) Training Process:

Step 1. Sample dataset establishment: The training sample data set is established by simply sampling and intercepting the data obtained from the simulation experiment.

Step 2. Feature extraction: The WPT is used to process the normal and fault sample data to get the initial feature data of the training sample set.

Step 3. The GcForest initialization: The internal structure parameters of the multi-grained scanning model are defined based on the specific features. The tuning range of the internal structure parameter is set at the same time as given in TABLE II.

Step 4. Model training: The preliminary feature data sample set is used to form the Gcforest model. The model adaptively determines the number of cascaded forest layers and produces the current cross validation accuracy.

Step 5. Model optimizing: Based on the precision generated by Step 3. , The Grid Search optimizer is used to update the internal structure setting of the cascading forest. Until the optimal model is obtained. The Optimized GcForest-based fault diagnosis model is constructed.

2) Testing Process:

Step 1. The test sample set is established by the same method as the training set.

Step 2. The preliminary feature data of the test sample set are extracted using the same method as the training set.

Step 3. The optimal fault diagnosis model based on the Gc-Forest is used to classify the test feature set, and the fault isolation result is obtained.

IV. SIMULATION RESULT ANALYSIS

A. Simulation Setup and Data Acquisition

The above-mentioned four-rotor UAV model is constructed under the simulation environment. The conditions for simulating the standard condition are as follows: the initial position is 0, the initial velocity is 0, the Euler angle is 0. The tracking signal is a pitch angle step signal with an amplitude of $10°$. The noise is Gaussian noise, with an average of 0 and a variance of $0.001°$. The simulation time is 5s and the fault injection time is 3s.

The faults are considered with the used of the 6-axis attitude sensor MPU6050^{TM}. By integrating accelerometer, gyroscope and digital motion processor, MPU6050^{TM} can accurately measure the acceleration, angular velocity and attitude angle of four-rotor UAV [28]. The parameters for each fault model are defined as follows: $\alpha_1 = 2°, \alpha_2 = 5°, k_1 = 0.7, \delta_1 = 70°$; $\dot{\alpha}_1 = 5°/s, \alpha_2 = 1°/s, \delta_2 = 10°/s$; $c_1 = 20$rad/s$, k_2 = 0.9, \delta_3 = -500$rad/s. The simulation result drawn in Fig. 5 shows that: (1) the designed controller can realize the attitude tracking of the four-rotor UAV; (2) the fault signals are different, yet easily masked by noise, so it is suitable for data-based fault diagnosis methods.

The amplitude of the tracking signal is set to 15°, 20° and 25° for the test condition. The sampling time is defined as $T =$ and the interception time is as $[2.5, 5]$ s. 500 sets of simulated data are obtained for each fault model. The standard condition data are split into testing and training data at a ratio of 1:1.

B. Data Preprocessing

The features of the signals observed by sensors are extracted. Where db2 wavelet is used for a three-layer WPT processing. The sensor signal has a constant value in the ideal normal state. To eliminate the coverage of the fault energy by the large high-frequency energy, nodes 2-8 are selected for energy feature consideration. As the actuator fault node energy shown in Fig. 6, the energy eigenvalues of the different fault are different in each frequency band. The energy features are similar in high-frequency nodes, but quite different at low-frequency ones. In this way, the feasibility and efficiency of the extraction of energy feature based on the WPT are proven.

C. Comparative Analysis of Parameter Optimization

The Grid Search algorithm is applied to optimize the internal structure parameters of cascade forest. Grid search is an automatic exhaustion method. According to the given parameter range, all possible parameter set is traversed computed. The best parameter set is therefore selected as the optimal solution. In order to demonstrate the superiority of the optimization

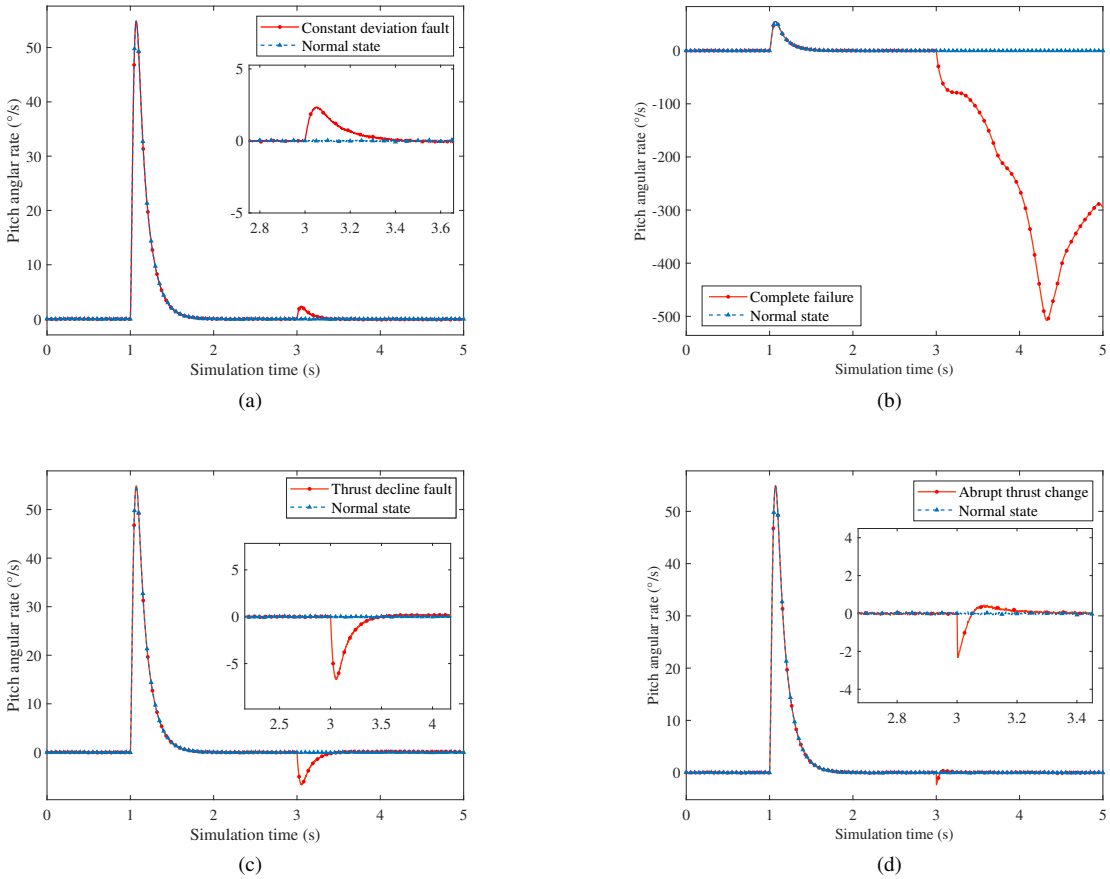

Fig. 5. The pitch angular rate response of four-rotor UAV with actuator fault. (a) constant deviation fault. (b) complete failure. (c) thrust decline fault. (d) abrupt thrust change.

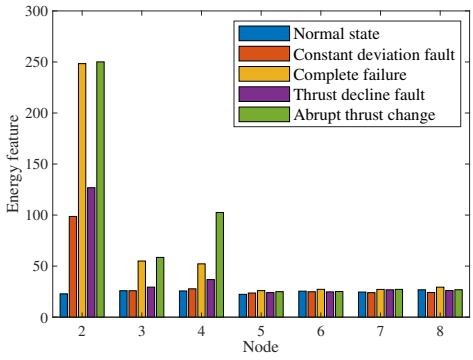

Fig. 6. The WPT node energy value of four-rotor UAV with the actuator fault.

method, the comparison parameters are defined. The results of parameter optimization and comparison set are given in TABLE III. For simplicity, the Gcforest built by comparison and optimal parameters are used to diagnose the actuator fault. Where the labels 0, 1, 2, 3, 4 represent the normal sate, the constant deviation fault, the complete failure, the thrust decline fault and the abrupt thrust change, respectively. As results

TABLE III
THE INTERNAL STRUCTURE PARAMETER OF THE CASCADE FOREST

	Optimum Value	**Comparison Value**
N_e	10	5
D_{max}	3	1
S_{min}	80	80
L_{min}	10	10

show in the Fig. 7a and Fig. 7b, a higher diagnosis accuracy is achieved by the optimal GcForest algorithm. Heretofore, the optimized fault diagnosis model based on Gcforest is constructed.

D. Comparative Analysis of Fault Diagnosis

Once the optimal fault diagnosis model is formed, the testing set is used to assess fault isolation performance. The parameters of the RF-based fault diagnosis model are defined as the optimal parameters obtained in the previous section. The diagnosis results of different faults are given in TABLE IV.

By comparing the results in Fig. 7b, Fig. 7c and TABLE IV, some conclusions are reached. Although the accuracy of the

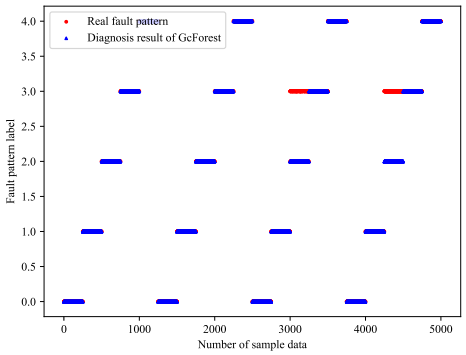

(a)

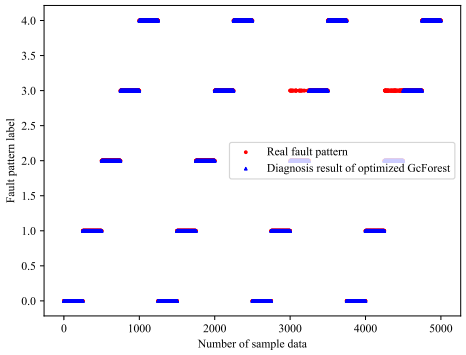

(b)

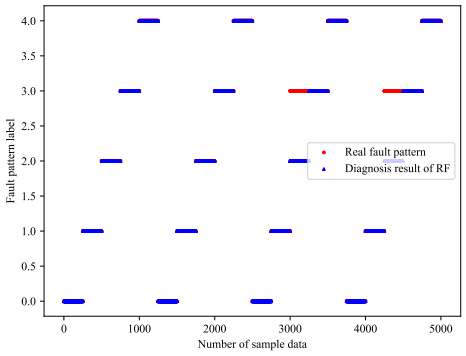

(c)

Fig. 7. Fault diagnosis result of the actuator fault. (a) fault diagnosis result of the GcForest. (with accracy of 92.96%) (b) fault diagnosis result of the optimized GcForest. (c) fault diagnosis result of the RF.

optimized GcForest-based fault diagnosis method is lower with the actuator and composite fault, it is still much better than the RF-based method. The possible reason is analyzed as follows: when the angular rate signal is used as the representation of the rotor speed, the integral operation is required. This operation will replace the high-frequency component of the sudden change signal with low-frequency components of the slow change signal. As a result, the sensitivity of energy features extracted by WPT to abrupt faults is weakened.

Moreover, most of the misdiagnosis was focused on the test condition with the tracking signal altitude of 20 and 25. The result shows that the proposed method can tolerate a certain changes in the operating condition of the four-rotor UAV. It also demonstrates that GcForest has better generalization performance under different flight conditions.

TABLE IV
FAULT DIAGNOSIS ACCURACY FOR DIFFERENT FAULTS

Fault Type		The Optimized GcForest Algorithm	The RF Algorithm
Sensor Fault	***Angle sensor***	99.50%	91.18%
	Angular rate sensor	100%	91.97%
Actuator Fault		98.08%	92.06%
Composite Fault		98.40%	93.08%

TABLE V
THE FAULT SIZE OF THE ANGLE SENSOR FAULT

Fault Label	Scenario 1	Scenario 2	Scenario 3	Scenario 4
1(°)	2	3	4	5
2(°)	2	3	4	5
3(%)	60	70	80	90
4(°)	60	70	80	90

E. Comparative Analysis of Fault Diagnosis Under Different Fault Size

The features for the fault diagnosis are derived from the signal data, making the amplitude and classification results closely related. But in the practical application process, the fault diagnosis system is expected to be able to diagnose the fault with a certain range of severity. For this reason, we diagnose the angle sensor fault and actuator fault with different fault size signals. Among them, 8 scenarios are listed in TABLE V and TABLE VI, and the fault diagnosis results using different diagnosis methods are given in TABLE VII. The results show that RF method and optimized GcForest method are likely to be confused and misdiagnosed in the face of faults with the same type but different sizes. However, the proposed method has an obvious priority and greater robustness.

V. CONCLUSION

In this paper, the GcForest algorithm is applied to the sensor, actuator and composite fault diagnosis of the four-rotor UAV. The WPT is used to extract features that reflect fault information from small samples of the sensor signal. Using

TABLE VI
THE FAULT SIZE OF THE ACTUATOR FAULT

Fault Label	Scenario 5	Scenario 6	Scenario 7	Scenario 8
1(rad/s)	20	30	40	50
2(rand/s)	0	0	0	0
3(%)	60	70	80	90
4(rand/s)	-400	-500	-600	-700

TABLE VII
FAULT DIAGNOSIS RESULT OF FAULT WITH VARYING FAULT SIZE

	Random Forest	Optimized GcForest
The Angle Sensor Fault	92.88%	95.82%
The actuator Fault	94.40%	99.14%

the GcForest algorithm, the mapping from fault feature space to fault pattern space is realized to diagnose faults. In addition, the Grid Search algorithm is applied to form the optimal fault diagnosis model. The simulation results show that the proposed algorithm can perform the fault diagnosis of the four-rotor UAV, with superiority and a strong generalization capability.

REFERENCES

[1] H. Lu, T. Fan, P. Ghimire, and L. Deng, "Experimental evaluation and consistency comparison of uav multispectral minisensors," *Remote Sens.*, vol. 12, no. 16, p. 2542, 2020.

[2] Z. Yijing, Z. Zheng, Z. Xiaoyi, and L. Yang, "Q learning algorithm based uav path learning and obstacle avoidence approach," in *2017 36th Chinese Control Conf. (CCC)*. IEEE, 2017, pp. 3397–3402.

[3] G. Iannace, G. Ciaburro, and A. Trematerra, "Fault diagnosis for uav blades using artificial neural network," *Robotics*, vol. 8, no. 3, p. 59, 2019.

[4] M. A. Al Mashhadani, "Optimal control and state estimation for unmanned aerial vehicle under random vibration and uncertainty," *Meas. Control*, vol. 52, no. 9-10, pp. 1264–1271, 2019.

[5] L. Zuo, L. Yao, and Y. Kang, "Uio based sensor fault diagnosis and compensation for quadrotor uav," in *2020 Chinese Control Decis. Conf. (CCDC)*. IEEE, 2020, pp. 4052–4057.

[6] Z. Zheng and X. Guanping, "Evolution analysis of a uav real-time operating system from a network perspective," *Chinese J. Aeronaut.*, vol. 32, no. 1, pp. 176–185, 2019.

[7] N. Kerle, F. Nex, M. Gerke, D. Duarte, and A. Vetrivel, "Uav-based structural damage mapping: A review," *ISPRS Int. J. Geo-Inf.*, vol. 9, no. 1, p. 14, 2020.

[8] Y. Zhong, W. Zhang, Y. Zhang, J. Zuo, and H. Zhan, "Sensor fault detection and diagnosis for an unmanned quadrotor helicopter," *J. Intell. Rob. Syst.*, vol. 96, no. 3, pp. 555–572, 2019.

[9] Q. Miao, J. Wei, J. Wang, and Y. Chen, "Fault diagnosis algorithm based on adjustable nonlinear pi state observer and its application in uav fault diagnosis," *Algorithms*, vol. 14, no. 4, p. 119, 2021.

[10] R. Venkataraman, P. Bauer, P. Seiler, and B. Vanek, "Comparison of fault detection and isolation methods for a small unmanned aircraft," *Control Eng. Pract.*, vol. 84, pp. 365–376, 2019.

[11] C. Chen, L. Zhang, J. Wang, and J. Zhang, "Application of fault diagnosis expert system for unmanned vehicle safety," in *IOP Conf. Ser.: Mater. Sci. Eng.*, vol. 608, no. 1. IOP Publishing, 2019, p. 012015.

[12] S. Y. Wong, C. W. C. Choe, H. H. Goh, Y. W. Low, D. Y. S. Cheah, and C. Pang, "Power transmission line fault detection and diagnosis based on artificial intelligence approach and its development in uav: A review," *Arabian J. Sci. Eng.*, pp. 1–27, 2021.

[13] X. Y. Zhang, D. Towey, T. Y. Chen, Z. Zheng, and K. Y. Cai, "A random and coverage-based approach for fault localization prioritization," in *2016 Chinese Control Decis. Conf. (CCDC)*. IEEE, 2016, pp. 3354–3361.

[14] H. Wang, C. Huang, H. Yu, J. Zhang, and F. Wei, "Method for fault location in a low-resistance grounded distribution network based on multi-source information fusion," *Int. J. Electr. Power Energy Syst.*, vol. 125, p. 106384, 2021.

[15] M. Kordestani, M. F. Samadi, M. Saif, and K. Khorasani, "A new fault diagnosis of multifunctional spoiler system using integrated artificial neural network and discrete wavelet transform methods," *IEEE Sens. J.*, vol. 18, no. 12, pp. 4990–5001, 2018.

[16] Z. Jin, Q. Han, K. Zhang, and Y. Zhang, "An intelligent fault diagnosis method of rolling bearings based on welch power spectrum transformation with radial basis function neural network," *J. Vib. Control*, vol. 26, no. 9-10, pp. 629–642, 2020.

[17] Y. Li, Y. Yang, X. Wang, B. Liu, and X. Liang, "Early fault diagnosis of rolling bearings based on hierarchical symbol dynamic entropy and binary tree support vector machine," *J. Sound Vib.*, vol. 428, pp. 72–86, 2018.

[18] D. Guo, M. Zhong, H. Ji, Y. Liu, and R. Yang, "A hybrid feature model and deep learning based fault diagnosis for unmanned aerial vehicle sensors," *Neurocomputing*, vol. 319, pp. 155–163, 2018.

[19] S. Ma, M. Chen, J. Wu, Y. Wang, B. Jia, and Y. Jiang, "Intelligent fault diagnosis of hvcb with feature space optimization-based random forest," *Sensors*, vol. 18, no. 4, p. 1221, 2018.

[20] Z. Zhou and J. Feng, "Deep forest," *Natl. Sci. Rev.*, vol. 6, no. 1, pp. 74–86, 2019.

[21] G. Hu, H. Li, Y. Xia, and L. Luo, "A deep boltzmann machine and multi-grained scanning forest ensemble collaborative method and its application to industrial fault diagnosis," *Comput. Ind.*, vol. 100, pp. 287–296, 2018.

[22] Q. Liu, H. Gao, Z. You, H. Song, and L. Zhang, "Gcforest-based fault diagnosis method for rolling bearing," in *2018 Prognos. Sys. Health Manage. Conf. (PHM-Chongqing)*. IEEE, 2018, pp. 572–577.

[23] G. Giacoppo, O. Barbera, N. Briguglio, F. Cipitì, M. Ferraro, G. Brunaccini, E. Erdle, and V. Antonucci, "Thermal study of a sofc system integration in a fuselage of a hybrid electric mini uav," *Int. J. Hydrogen Energy*, vol. 42, no. 46, pp. 28 022–28 033, 2017.

[24] J. Yaghoobi, A. Alduraibi, D. Martin, F. Zare, D. Eghbal, and R. Memisevic, "Impact of high-frequency harmonics (0–9 khz) generated by grid-connected inverters on distribution transformers," *Int. J. Electr. Power Energy Syst.*, vol. 122, p. 106177, 2020.

[25] A. Othman, N. Hamzah, Z. Hussain, R. Baharudin, A. D. Rosli, and A. I. C. Ani, "Design and development of an adjustable angle sensor based on rotary potentiometer for measuring finger flexion," in *2016 6th IEEE Int. Conf. Control Syst. , Comput. Eng. (ICCSCE)*. IEEE, 2016, pp. 569–574.

[26] Y. Shi, J. Zhang, J. Jiao, R. Zhao, and H. Cao, "Calibration analysis of high-g mems accelerometer sensor based on wavelet and wavelet packet denoising," *Sensors*, vol. 21, no. 4, p. 1231, 2021.

[27] Q. Yao, M. Wang, Y. Chen, W. Dai, Y. F. Li, W. W. Tu, Q. Yang, and Y. Yu, "Taking human out of learning applications: A survey on automated machine learning," *arXiv preprint arXiv:1810.13306*, 2018.

[28] A. Hassan, Z. Liu, S. S. Abbas, Y. Li, L. Wang, X. Liu, and P. Zhao, "Statistical scheme for fault detection using arduino and mpu 6050," in *2019 Prognos. Sys. Health Manage. Conf. (PHM-Qingdao)*. IEEE, 2019, pp. 1–7.